SAND2017-3118J

Plasma Parameters from Reentry Signal Attenuation

T. K. Statom, *Senior Member, IEEE*

***Abstract*— This article presents the application of a theoretically developed method that provides plasma parameter solution space information from measured RF attenuation that occurs during reentry. The purpose is to provide reentry plasma parameter information from communication signal attenuation. The theoretical development centers around the attenuation and the complex index of refraction. The methodology uses an imaginary index of refraction matching algorithm with a tolerance to find suitable solutions that satisfy the theory. The imaginary matching terms are then used to determine the real index of refraction resulting in the complex index of refraction. Then a filter is used to reject nonphysical solutions. Signal attenuation based plasma parameter properties investigated include the complex index of refraction, plasma frequency, electron density, collision frequency, propagation constant, attenuation constant, phase constant, complex plasma conductivity and electron mobility. RF plasma thickness attenuation is investigated and compared to the literature. Similar plasma thickness for a specific signal attenuation can have different plasma properties.**

***Index Terms*—Index of refraction, matching and filtering algorithm, plasma diagnostics, plasma sheath, propagation constant**

I. Introduction

REENTRY plasma can be investigated by using nonmagnetized collisional plasma theory. The fundamentals of nonmagnetized collisional plasmas can be found in texts [1] [2]. The plasma layer properties can be considered in two ways, as uniform or the mean value across the plasma. Nonmagnetized collisional plasmas being used as a basis to investigate reentry plasma is documented in the literature[3] [4] [5]. These articles demonstrate the relationship between electron density and plasma attenuation. The literature further refines electron density reentry plasma [6-14]. Reentry attenuation properties have been published as well [3] [5][14] [15][16]. The approach described here proceeds from the fundamentals in the literature [3][4][5] in a direction to further exploit the solution space by using the imaginary part of the complex index of refraction through a matching algorithm and physical constraint filter. The purpose is to provide reentry plasma parameter information from communication signal attenuation. The method results are compared with what is in the literature to evaluate its viability and consistency.

The approach to investigate the plasma parameters are based upon the theory being applied to a matching algorithm with tolerance. The matching algorithm uses a specific signal attenuation for a plasma thickness in order to determine the imaginary part of the complex index of refraction. Iteration across the ratio of the plasma frequency to the RF frequency (ω_p^2/ω^2 = X, ω_p/ω = X1) and the ratio of the collision frequency to the RF frequency (ν_m/ω = Z) are used in order to investigate the solutions of the plasma parameters. The results are filtered using the physical constraint that the group velocity must be less than the speed of light.

Manuscript received March 1, 2017. This work was supported by the U.S. Department of Energy's National Nuclear Security Administration under Contract DE-AC04-94AL85000.

The author is with the Sandia National Laboratories, Albuquerque, NM 87123 (e-mail: tstatom@sandia.gov).

II. Theory

RF attenuation in a nonmagnetized collisional plasma is a function of the RF frequency. The angular frequency ω (rad/s) is 2πf, where f (Hz) is the frequency. The electric field for a plane electromagnetic attenuating traveling wave can be represented as in equation (1).

$$E = E_o e^{-\alpha z} e^{j(\omega t - \beta z)} \tag{1}$$

Where α is the attenuation constant, β is the phase constant, j is the imaginary unit, z is the propagation length and t is time. Equation (2) represents the relationship between the propagation constant, complex dielectric constant ($\varepsilon=\varepsilon_o\varepsilon_r$, ε_o is the permittivity of free space and ε_r is the relative permittivity) and the complex index of refraction [3].

$$\gamma = \alpha + j\beta = j\sqrt{\varepsilon_r}\frac{\omega}{c} = jn\frac{\omega}{c} = j\left(n_r - jn_j\right)\frac{\omega}{c} = (jn_r + n_j)\frac{\omega}{c} \tag{2}$$

Where γ is the propagation constant, n is the complex index of refraction, n_r is the real variable of the complex index of refraction, and n_j is the imaginary variable of the complex index of refraction. Equation (2) shows the relationship between the attenuation constant and the imaginary part of the complex index of refraction and the phase constant and the real part of the complex index of refraction. Equation (3) displays the relationship specifically.

$$\alpha = n_j\frac{\omega}{c}\ , \beta = n_r\frac{\omega}{c} \therefore n = \frac{c}{\omega}(\beta - j\alpha) \tag{3}$$

The wave number is given by equation (4) [2].

$$k = \frac{1}{c}\left(\omega^2 - \frac{{\omega_p}^2}{1+j(Z)}\right)^{1/2} \quad (4)$$

Where k is the wavenumber, c is the speed of light, ω_p is the plasma frequency, and ν_m is the electron momentum collision frequency. The plasma frequency (taken as the electron plasma frequency) is expressed in equation (5).

$$\omega_p = \left(\frac{n_e e^2}{\varepsilon_o m_e}\right)^{1/2} \quad (5)$$

Where n_e is the electron density, e is the fundamental charge, and m_e is the electron mass. The index of refraction is the wavenumber times the speed of light divided by the radial frequency ($n=kc/\omega$). The relative permittivity can be expressed as in equation (6).

$$\sqrt{\varepsilon_r} = \left[1 - \frac{X}{1+(Z)^2} + j\frac{X(Z)}{1+(Z)^2}\right]^{\frac{1}{2}} \quad (6)$$

In equation (6) the second term in the brackets can be expressed as in equation (7).

$$N = \frac{X}{1+(Z)^2} \quad (7)$$

Replacing equation (7) into equation (6) gives equation (8).

$$\sqrt{\varepsilon_r} = n = [1 - N + jN(Z)]^{\frac{1}{2}} \quad (8)$$

Considering the complex number in the z-plane, the complex radius or magnitude of ε_r is given by equation (9).

$$R = \sqrt{(1-N)^2 + (N(Z))^2} \quad (9)$$

With the complex angle for ε_r given by equation (10).

$$\theta = \tan^{-1}\left(\frac{N(Z)}{(1-N)}\right) \quad (10)$$

The roots of the relative permittivity or the index of refraction is based on De Moivre's theorem and is expressed in equation (11) and equation (12).

$$n1 = n_r - jn_j = R^{\frac{1}{2}}\left\{\cos\frac{\theta}{2} + j\sin\frac{\theta}{2}\right\} \quad (11)$$

$$n2 = R^{\frac{1}{2}}\left\{\cos\frac{\theta+2\pi}{2} + j\sin\frac{\theta+2\pi}{2}\right\} \quad (12)$$

The real part of the phase velocity is given in equation (13).

$$v_\phi = \frac{c}{Re[n]} = \frac{c}{n_r} \quad (13)$$

The real part of the group velocity is given in equation (14).

$$v_g = \frac{d\omega}{dk} \cong \frac{c}{Re[n]+\omega\left[Re\left[\frac{\partial n}{\partial \omega}\right]\right]} = \frac{c}{n_r+\omega\left[Re\left[\frac{\partial n}{\partial \omega}\right]\right]} \quad (14)$$

The derivative in equation (14) can be expressed as in equation (15).

$$\frac{\partial n}{\partial \omega} = \frac{{\omega_p}^2(2\omega + j\nu_m)}{2(\omega^2 + j\omega\nu_m)^2\left(1 - \frac{{\omega_p}^2}{\omega^2+j\omega\nu_m}\right)^{\frac{1}{2}}} \quad (15)$$

Recognizing that equation (15) can also be written as in equation (16).

$$\frac{\partial n}{\partial \omega} = \frac{{\omega_p}^2(2\omega + j\nu_m)}{2(\omega^2 + j\omega\nu_m)^2(n_r - jn_j)} \quad (16)$$

Multiplying the terms in the denominator except the 2 and collecting terms, leaves V+jW, where V and W are expressed in equation (17) and equation (18).

$$V = n_r(\omega^4 - \omega^2{\nu_m}^2) + n_j(2\omega^3\nu_m) \quad (17)$$

$$W = n_j(\omega^2{\nu_m}^2 - \omega^4) + n_r(2\omega^3\nu_m) \quad (18)$$

Taking the complex conjugate (V-jW), the real part of the partial derivative expressed in equation (16) is given in equation (19) and used in equation (14) to evaluate the group velocity.

$$Re\left[\frac{\partial n}{\partial \omega}\right] = \frac{{\omega_p}^2(2\omega V + \nu_m W)}{2(V^2+W^2)} \quad (19)$$

The plasma conductivity [20] can be represented by taking the complex conjugate and separating the real and imaginary parts of the complex plasma conductivity as in equation (20).

$$\sigma_p = \frac{\varepsilon_o{\omega_p}^2\nu_m}{{\nu_m}^2+\omega^2} - j\frac{\varepsilon_o{\omega_p}^2\omega}{{\nu_m}^2+\omega^2} \quad (20)$$

The ratio of the drift velocity to the electric field or electron mobility [21] is represented as in equation (21).

$$\mu_e = \frac{e}{m_e\nu_m} \quad (21)$$

III. Method

The relationship between the attenuation constant and the imaginary part of the complex index of refraction as in equation (3) with the units of dB (recall the relationship between Np and dB following the description in [3]) are considered in Equation (22). This is done because α is in Nepers per meters but the signal attenuation is measured in dB.

$$\alpha\left(\frac{Np}{m}\right) = n_j\frac{\omega}{c}, \left\{1\ Np = \frac{20}{ln10}(dB)\right\} \quad (22)$$

The Attenuation in dB is given in equation (23) converting from Np to dB as in equation (22).

$$A(dB) = \alpha z = \alpha L \quad (23)$$

Where L is plasma thickness or length. The attenuation equation can be expressed [3] by replacing the attenuation constant with the imaginary part of the complex index of refraction according to equation (22) and displayed in equation (24). In the equation the attenuation A is held constant and L is varied to investigate the attenuation constant through the imaginary part of the complex index of refraction. The negative sign used here incorporates the negative sign in the complex index of refraction representation in equation (2).

$$-Ln_j = -\frac{ln10Ac}{20\omega} \tag{24}$$

Knowing the value of equation (24) from the attenuation, the plasma length is varied to find an array $(n_j)_i$ which is consistent (based on the theoretical assumptions) with a set of lengths L_i, the plasma thickness. The imaginary part of the complex index of refraction from this is in equation (25). The negative value in equation (25) will match the negative values for the imaginary part of n1 in equation (11), which is equivalent to sinθ/2 being negative. This follows for equation (12) as well. It should be remembered that $-n_j=-\alpha(c/\omega)$ from equation (3), and therefore $\alpha=-(-n_j)(\omega/c)$.

$$(-n_j)_i = -\frac{Ln_j}{L_i} \tag{25}$$

Reformulating the complex index of refraction equation expressed in equation (6) leads to equation (26).

$$(n)_{m,p} = (n_r)_{m,p} - j\left(n_j\right)_{m,p} = \left[1 - \frac{(X)_m}{1+(Z)_p{}^2} + j\frac{(X)_m(Z)_p}{1+(Z)_p{}^2}\right]^{\frac{1}{2}} \tag{26}$$

Equation (26) is developed similarly as equation (6) through equation (12). By varying X1 (recall that $X1^2=X$) and Z a matrix of possible $(n)_{m,p}$ are determined. X1 may represent 10 to 1000 for example, while Z may represent .001 to 5 for example. The results are put into a matching algorithm where results ($(n_j)_{o,p}$) that meet the following threshold condition in equation (27) are kept as viable solutions.

$$\left|(-n_j)_i - (-n_j)_{m,p}\right| < \Delta n_j \tag{27}$$

The complex index of refraction expressed in equation (2) and equation (11) has a positive real value and a negative imaginary value. This places it in the fourth quadrant of the complex plane, which is equivalent to sinθ/2 being negative in equation (11). This provides the possible solutions for the complex index of refraction based upon the attenuation. X1 and Z are retained as well. Knowing the RF frequency, the plasma frequency, electron density, collision frequency, and phase velocity can be found for the specified conditions. The group velocity can then be established by using equation (14) and equation (19). The plasma conductivity and electron mobility can be found under the specified conditions as well. Because the group velocity must be less than the speed of light, a filter is multiplied across the solution space that meets the threshold condition. A physical filter is used on the results matrix from the threshold test, where all values with $V_g < c$ are retained.

The physical filter is multiplied element by element to the complex index of refraction so that only results that can meet equation (26) at the specified threshold given by equation (27) and that are physically possible are retained. Zeros are taken out of the matrix and the solutions are put into a vector. With the real and imaginary parts of the index of refraction solution space determined, the attenuation constant and phase constant solution space can be evaluated from equation (3). Knowing the terms from the propagation constant, equation (1) can be normalized into the format of equation (28).

$$\frac{E}{E_o} = e^{-\alpha z}Re\left[e^{j(\omega t-\beta z)}\right] \tag{28}$$

The underlying electron density distribution across the plasma length can be investigated as uniform or according to the bi-Gaussian plasma electron density distribution model [15][17] also known as the electron density parametrized model[18]. This model has a similar shape to those based upon nonlinear statistics applied to equilibrium chemistry and experimental turbulent characteristics [19]. Here this is used where the mean of the distribution across the plasma thickness matches what was determined by the method in this paper. Equation (29) displays the representation of this electron density distribution model across the plasma thickness or length.

$$n_e(l) = \begin{cases} max(n_e)e^{(-x_1(l-l_B)^2)} & (0 < l < l_B) \\ max(n_e)e^{(-x_2(l-l_B)^2)} & (l_B < l < L) \end{cases} \tag{29}$$

Where $\max(n_e)$ is the peak value of the electron density, x_1 and x_2 are constants, l is the length variable across the plasma, l_B is the location of $\max(n_e)$ and L is the total plasma length or thickness. The terms in equation (29) are selected so that the mean electron density, mean attenuation constant and mean phase constant across the plasma length are those approximated from the matching and filtering algorithm results. The collision frequency is taken as a uniform distribution across the plasma length approximating what is in the literature [5]. Equation (9) through equation (12) are used to determine the complex index of refraction and therefore the attenuation and phase constant based upon ω_p (from $n_e(l)$ in equation (29)), ν_m from the match and filtering algorithm, and ω. The constants in equation (29) are changed so that the mean of the electron density, attenuation constant and phase constant across the plasma length are approximately equal to the terms found by the matching and filtering algorithm. This means that the total attenuation and phase change across the plasma length is the same for the uniform distribution as it is for the bi-Gaussian distribution.

IV. Results

In Table I an example algorithm set-up follows for the variables previously mentioned using equation (11) and equation (12) for the threshold match. For Table I equation (11) results were found, however, no solutions were found for

equation (12). The first root (equation (11)) found matching results and the second one (equation (12)) did not. The plasma length range and attenuation was selected based upon expected reentry plasma density. The X1 and Z ranges were selected to provide solutions consistent with some reentry plasma and Δn_j was selected to provide matching error bounds.

TABLE I
Matching and Filtering Algorithm Set-Up

Frequency (ω)	2 GHz (1.256 x 10^{10} rad/s)
RF Attenuation	40 dB
Plasma Length (L_i)	0.01 cm to 100 cm by .01 cm steps
X1 (ω_p/ω)	10 to 100 by steps of 1
Z (ν_m/ω)	0.2 to 2 by .01 steps
Δn_j	0.00005

With the setting for X1 and Z, the collision and plasma frequency parameter space investigated are specified in Table I. This is done to investigate the variability of other parameters (i.e., attenuation constant and phase constant) evaluated from the method used in this paper. Decreasing the step size for X1 and Z in Table I increases the number of solutions obtained across the plasma length. The frequency, attenuation, plasma length, ranges, step size and threshold listed in Table I yields 34 solutions. Tables II and III show the results. In the tables the plasma lengths L are those determined from the matching and filtering algorithm and therefore do not have uniform spacing. Table II and III displays a result with plasma length of 2.17 cm that has two solutions. The attenuation is the same (40 dB), the length is the same (2.17 cm), and therefore the attenuation constant is the same (212.22 Np/m), however, the phase constants are different as are the plasma frequency and collision frequency. For the two 2.17 cm cases the values can be placed in equations (9-11) to obtain the same imaginary index of refraction representation confirming the matching and filtering algorithms self-consistency performance. Table II also shows for the same plasma lengths (2.17 cm) and attenuation constants, the phase constant may be twice as large causing greater phase change across the plasma for the same signal attenuation. This also means that the real part of the complex index of refraction are not unique for a specific attenuation and plasma length whereas the imaginary part is.

From Table III it can be seen that when the collision frequency is larger than the propagation frequency then the group velocity is larger than the phase velocity and when the propagation frequency is larger than the collision frequency then the group velocity is smaller than the phase velocity. This holds for the table except the 2.22 cm solution where the collision frequency and propagation frequency are the closest suggesting a transition region. Investigating this further shows that for this method when the propagation frequency is greater than the collision frequency the phase velocity is greater than the group velocity. When the collision frequency is greater than the propagation frequency but within 8% the phase velocity is greater than the group velocity. When the collision frequency is greater than the propagation frequency by 8% the group velocity is larger than the phase velocity.

TABLE II
MATCHING AND FILTERING ALGORITHM RESULTS

L (cm)	α (Np/m)	β (rad/m)	n_e ($1/cm^3$)	μ_e ($m^2/(V\text{-}s)$)
0.48	959.41	1759.96	2.09E+14	9.06
0.59	780.54	1674.60	1.49E+14	11.80
0.89	517.43	853.47	6.05E+13	7.35
1.06	434.45	963.09	4.75E+13	12.43
1.11	414.88	1243.37	6.05E+13	18.73
1.37	336.14	1876.28	1.09E+14	37.96
1.63	282.52	1465.88	6.76E+13	35.12
1.74	264.66	1476.85	6.76E+13	37.96
1.86	247.59	490.85	1.43E+13	10.48
1.89	243.66	509.32	1.43E+13	11.42
2.11	218.25	1106.13	3.87E+13	34.26
2.12	217.22	577.97	1.43E+13	16.15
2.14	215.20	636.32	1.60E+13	18.48
2.17	212.22	459.99	1.11E+13	12.11
2.17	212.22	1154.43	4.15E+13	36.97
2.21	208.38	359.59	9.68E+12	8.21
2.22	207.44	474.69	1.11E+13	13.13
2.58	178.49	289.10	7.11E+12	7.28
2.62	175.77	729.25	1.78E+13	27.54
2.98	154.54	511.55	9.68E+12	21.28
3.08	149.52	257.88	4.94E+12	8.36
3.1	148.55	518.39	9.68E+12	22.66
3.32	138.71	528.47	9.68E+12	25.08
3.95	116.59	983.59	2.84E+13	58.53
3.97	116.00	455.32	7.11E+12	26.01
4.2	109.65	460.87	7.11E+12	28.09
4.82	95.54	379.94	4.94E+12	26.50
5.86	78.58	611.73	1.11E+13	54.03
5.88	78.32	393.18	4.94E+12	34.26
6.8	67.72	443.31	5.98E+12	45.31
8.19	56.23	405.11	4.94E+12	50.17
9.44	48.79	408.08	4.94E+12	58.53
10.2	45.15	452.13	5.98E+12	70.23
11.21	41.08	410.66	4.94E+12	70.23

In the cases of the same plasma lengths with different plasma properties, the determination of which specific solution is correct for an application would come from the collision frequency determined by the reentry aerodynamic properties of the gas. If the same length does not yield more than one solution, the collision frequency determined is consistent with the theory. The electron density solutions are in the 10^{12} to 10^{14} ($1/cm^3$) range for the Table I case. The electron mobility increases with decreasing collision frequency which comes from equation (21). The electron energy is not investigated. The gas properties are needed in order to investigate the electron energy due to momentum transfer from the gas neutrals. This investigation determined plasma properties that can be found under the theoretical

matching and filtering constraints from plasma length solutions and signal attenuation.

TABLE III
MATCHING AND FILTERING ALGORITHM RESULTS

L (cm)	ω_p (rad/s)	ν_m (rad/s)	v_ϕ (m/s)	v_g (m/s)
0.48	8.17E+11	1.95E+10	7.14E+06	8.97E+06
0.59	6.91E+11	1.50E+10	7.50E+06	7.98E+06
0.89	4.40E+11	2.40E+10	1.47E+07	2.06E+07
1.06	3.90E+11	1.42E+10	1.30E+07	1.34E+07
1.11	4.40E+11	9.42E+09	1.01E+07	7.87E+06
1.37	5.91E+11	4.65E+09	6.70E+06	3.85E+06
1.63	4.65E+11	5.03E+09	8.57E+06	5.03E+06
1.74	4.65E+11	4.65E+09	8.51E+06	4.89E+06
1.86	2.14E+11	1.68E+10	2.56E+07	2.95E+07
1.89	2.14E+11	1.55E+10	2.47E+07	2.69E+07
2.11	3.52E+11	5.15E+09	1.14E+07	6.72E+06
2.12	2.14E+11	1.09E+10	2.17E+07	1.86E+07
2.14	2.26E+11	9.55E+09	1.97E+07	1.55E+07
2.17	1.88E+11	1.46E+10	2.73E+07	2.86E+07
2.17	3.64E+11	4.78E+09	1.09E+07	6.30E+06
2.21	1.76E+11	2.15E+10	3.49E+07	4.66E+07
2.22	1.88E+11	1.34E+10	2.65E+07	2.62E+07
2.58	1.51E+11	2.43E+10	4.35E+07	6.16E+07
2.62	2.39E+11	6.41E+09	1.72E+07	1.10E+07
2.98	1.76E+11	8.29E+09	2.46E+07	1.77E+07
3.08	1.26E+11	2.11E+10	4.87E+07	6.48E+07
3.1	1.76E+11	7.79E+09	2.42E+07	1.69E+07
3.32	1.76E+11	7.04E+09	2.38E+07	1.58E+07
3.95	3.02E+11	3.02E+09	1.28E+07	6.79E+06
3.97	1.51E+11	6.79E+09	2.76E+07	1.80E+07
4.2	1.51E+11	6.28E+09	2.73E+07	1.72E+07
4.82	1.26E+11	6.66E+09	3.31E+07	2.14E+07
5.86	1.88E+11	3.27E+09	2.05E+07	1.10E+07
5.88	1.26E+11	5.15E+09	3.20E+07	1.88E+07
6.8	1.38E+11	3.90E+09	2.83E+07	1.56E+07
8.19	1.26E+11	3.52E+09	3.10E+07	1.68E+07
9.44	1.26E+11	3.02E+09	3.08E+07	1.63E+07
10.2	1.38E+11	2.51E+09	2.78E+07	1.45E+07
11.21	1.26E+11	2.51E+09	3.06E+07	1.59E+07

The complex index of refraction solutions are in the Fig.1 polar plot. The solutions are in the fourth quadrant as expected by the theory and method development. The real and the imaginary index of refraction values as a function of plasma length is displayed in Fig. 2. The real values are larger than the magnitude of the imaginary values. The complex magnitude of the imaginary index of refraction decreases with increasing plasma length which is consistent with the attenuation constant for 40 dB attenuation. The real index of refraction values do not follow this trend and therefore the phase constant does not either.

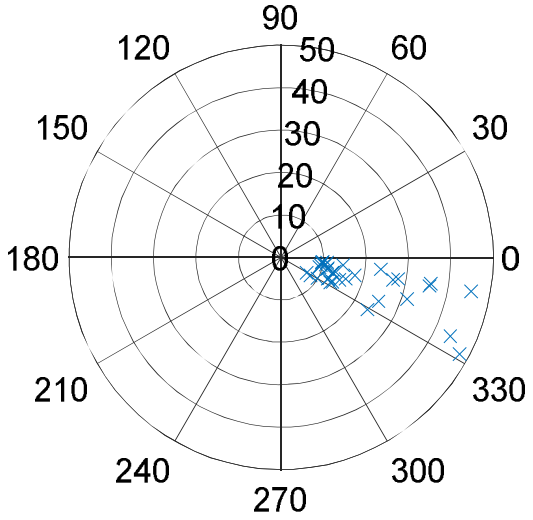


Fig. 1. Complex Index of Refraction Solutions Polar Plot.

A representation of the complex plasma conductivity is displayed in Fig. 3. The solutions for the complex plasma conductivity is in the fourth quadrant in the polar plot which is consistent with the theoretical representation in equation (20). In general from the polar plot the imaginary values are larger than the real values but not in all cases.

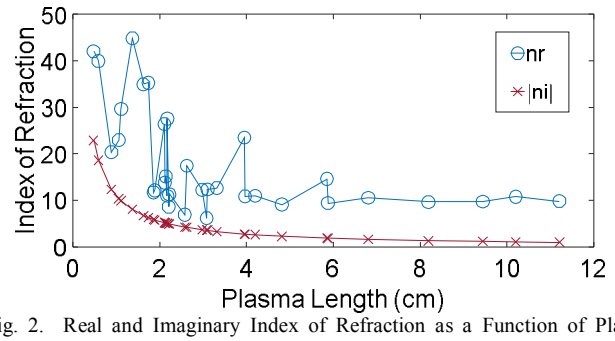


Fig. 2. Real and Imaginary Index of Refraction as a Function of Plasma Length.

The plasma conductivity generally decreases with increasing plasma length as shown in Fig. 4, however, this does not hold up for each case. At plasma lengths from around 4 cm to 11 cm the magnitude of the imaginary conductivity values are greater than the real values. This is not always the case at plasma lengths smaller than 4 cm.

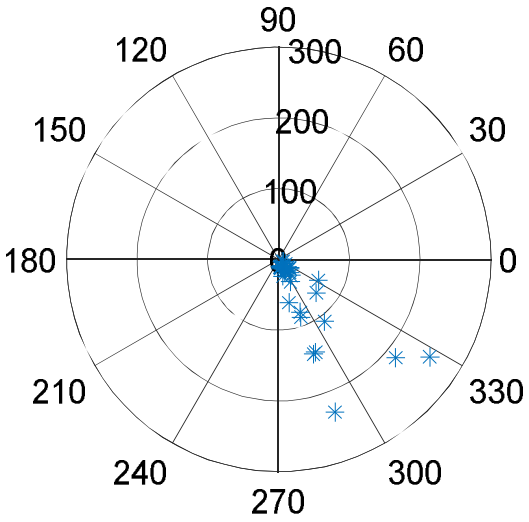


Fig. 3. The Complex Plasma Conductivity (1/Ω-m)

The group velocity and the phase velocity as a function of plasma length is displayed in Fig. 5. No group velocity values are greater than c, consistent with the filter. The medium is dispersive because the group and phase velocity are not equal. They are almost equal at plasma length 2.22 cm as in Table III.

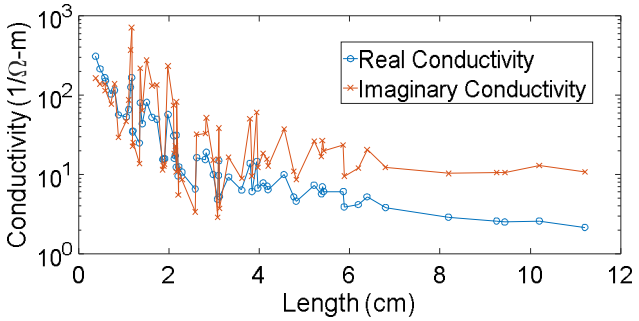


Fig. 4. The Real and Imaginary Plasma Conductivity as a Function of Plasma Length.

The E/Eo surface plot for a uniform distribution (electron density, propagation constant and phase constant) for the first L=2.17 cm solution in Table II is displayed in Figure 6. The plasma length and time shown display the field propagation in the plasma.

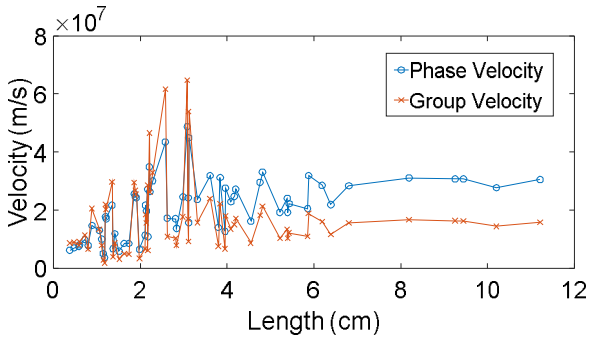


Fig. 5. Phase and Group Velocity as a Function of Plasma Length.

For a bi-Gaussian distribution, where the value for the electron density, attenuation constant and phase constant across the plasma length is approximated by their means. In Fig. 7 the terms in the bi-Gaussian equation are max(n_e)=1.24 x 10^{19} ($1/m^3$), L=2.17 cm, l_B=0.651 cm, x1=1.1 and x2=0.12. For the same time and space axis as in Fig. 6 the field is propagating slightly differently in the plasma with the bi-Gaussian distribution as it does in the uniform distribution. This is a representation of the first solution for L=2.17 cm.

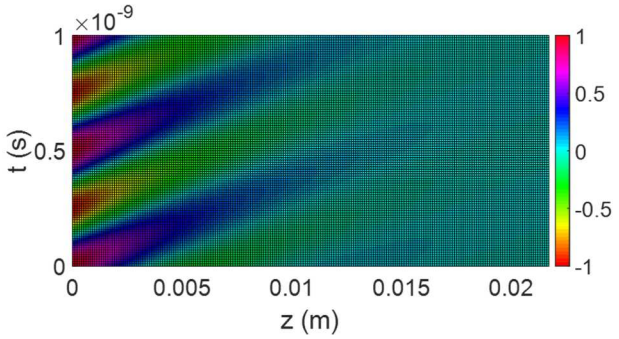


Fig. 6. E/Eo Uniform Distribution for L=2.17 cm first solution in Table II.

For the second solution for L=2.17 cm a surface plot of E/Eo for a uniform distribution is shown in Fig. 8. For the same time and space scale the field propagates through the plasma differently than the first solution for 2.17 cm with a uniform distribution.

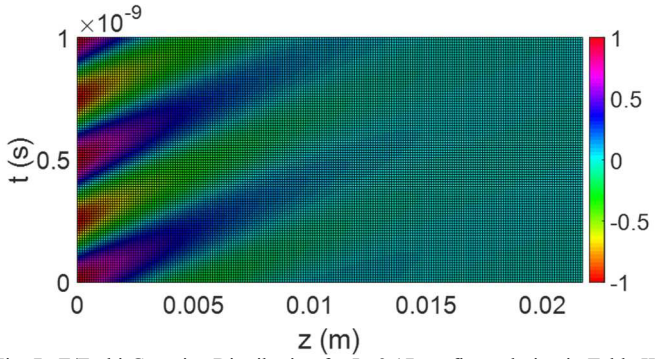


Fig. 7. E/Eo bi-Gaussian Distribution for L=2.17 cm first solution in Table II.

In this case it also propagates differently than the first solution for the first 2.17 cm case with a bi-Gaussian distribution.

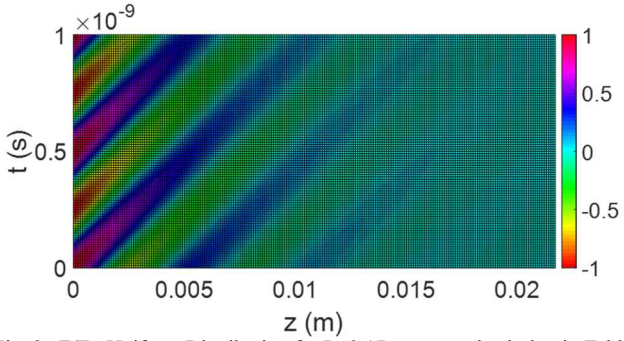


Fig. 8. E/Eo Uniform Distribution for L=2.17 cm second solution in Table II.

A bi-Gaussian for the second L=2.17 cm case is shown in Fig. 9. The terms in the bi-Gaussian equation are

max(n_e)=1.24 x 10^{19} (1/m^3), L=2.17 cm, l_B=0.651 cm, x1=0.7 and x2=0.09. For the same time and space axis as in Fig. 8 the field is propagating slightly differently in the plasma with the bi-Gaussian distribution than it does in the uniform distribution. The first solution propagation for the uniform and bi-Gaussian are similar but slightly different when compared to the second solution propagation for the uniform and bi-Gaussian which are also similar in comparison. This expresses different field propagation properties for the same attenuation. This is expected since the phase constant is different as is the real index of refraction that it comes from.

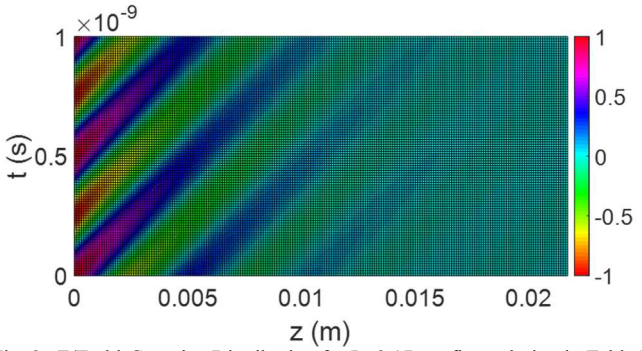


Fig. 9. E/Eo bi-Gaussian Distribution for L=2.17 cm first solution in Table II.

V. Discussion

The reentry plasma peak electron density that Kiel et. al [6] presented along the reentry body (1/cm^3) ranged from 10^{15} values near the nose cone to 10^9 at around 700 cm from the nose cone. At locations from 172 cm to 423 cm at boundary-layer thickness from 0 to ~10.5 mm the electron density ranges from 10^8 to 10^9 1/cm^3. This suggest that near the nose cone with the boundary layer thickness equivalent to the plasma thickness developed by this method there is good agreement with the first four or five solutions in Table II.

Reentry plasma electron density obtained by Kane [9] for an equilibrium sodium case (comes from the nose cone) for altitudes from 100 to 120 kft, is above 10^{12} but below 5 x 10^{12} 1/cm^3 with a trend increasing with decreasing altitude. This is consistent with values in the Table II results as well.

The values determined by Candler and MacCormack [11] for reentry plasma electron density (which applies numerical methods and compares to the RAM-C II flight test data) show that for numerical methods the centerline distance to nose cone radius ratios (x/R_N) from 0 to 9 have an electron density range from 10^{14} to 10^{11} 1/cm^3 at a free stream Mach number of 23.9 and an altitude of 61 km. At a free stream Mach number of 25.9 and an altitude of 71 km under the same ratio conditions an electron density range from 10^{13} to 10^{10} 1/cm^3 is presented. At a free stream Mach number of 28.3 and an altitude of 81 km an electron density range from 10^{12} to 10^9 1/cm^3 was given. The upper levels of these ranges or where the location is closer to the nose cone have electron densities in the range used by this method for a signal attenuation of 40 dB. It should be remembered, however, that this is for the purpose of investigating plasma parameters with a specific signal attenuation. This supports that the electron density in Table II and III are reasonable for some reentry plasma cases.

Using numerical solutions (Watkins and Blottner [13]) with an altitude of 34 km and a Mach number of 21.9 with x/R_N from 1 to 10 has an electron density range from 10^{15} to 10^{13} 1/cm^3, R_N is 0.254 cm. The lower end of this is in agreement with the application of this method, however, different X1 and Z ranges would yield different results, in other words Table I could be changed to investigate higher or lower electron density ranges depending on the attenuation and reentry plasma flow (length) conditions. They also show that at x/R_N of 200 and a y/R_N from 0 to 1.2 or (0 to 0.3 cm) boundary layer thickness (plasma length) the electron density ranges from 10^{11} to 10^6 1/cm^3, which is low for the results in Table II and the settings in Table I of this method. The variables in Table I could be varied to examine signal attenuation under these reentry plasma conditions.

Savion et. al [14] obtained reentry plasma electron density values by distance from the nose tip in the range of 10^{12} 1/cm^3. They presented a graph of plasma frequency as a function of plasma length with a specific signal attenuation. For the x=0.55m case, the peak plasma frequency is around 3.5 GHz and the plasma length is around 80 cm. The distribution is not uniform. The method developed here was tested against these results. Using the method described here for a uniform distribution an attenuation of 132.67 dB and a frequency of 1575.42 MHz a solution with plasma frequency of 3.17 GHz, collision frequency of 5.48 x 10^9 rad/s and a plasma length of 79.96 cm was found. A bi-Gaussian distribution was also investigated. The terms in the bi-Gaussian equation were max(n_e)=1.52 x 10^{17} (1/m^3), L=80 cm, l_B=18.67 cm, x1=0.0066 and x2=0.003, the collision frequency was the same as in the uniform distribution. The bi-Gaussian distribution was similar to the published plasma frequency as a function of plasma length. The attenuation across the plasma was only considered from complex index of refraction solutions that were in the fourth quadrant consistent with the theoretical development. This resulted in an attenuation of 128.64 dB. These cases show agreement with what is published.

VI. Conclusion

The purpose of this method is to provide reentry plasma parameter information from communication signal attenuation. The application of nonmagnetized collisional plasma theory to the complex index of refraction matching and filtering algorithm provide plasma parameter solutions under plasma thickness and signal attenuation constraints. The matching and filtering algorithm self-consistency has been confirmed by determining the same imaginary index of refraction for two cases with the same plasma length having different plasma properties and propagation characteristics. These cases demonstrate that having the same signal attenuation, plasma lengths and attenuation constants can result in a phase constant twice as large. The same signal attenuation with the same length of plasma may have different underlying plasma properties for the phase constant, collision frequency and plasma frequency. With a plasma frequency

greater than the propagation frequency the relationship between the collision frequency and the propagation frequency was explored. Using this method when the propagation frequency is greater than the collision frequency the phase velocity is greater than the group velocity. When the collision frequency is about the same as the propagation frequency the phase velocity is greater than the group velocity. When the collision frequency is much greater than the propagation frequency the group velocity is greater than the phase velocity. The electron density solutions are consistent with other published reentry plasma literature results. The approach taken here when compared to a literature case with a specific signal attenuation and plasma length determined solutions for plasma length, plasma frequency and attenuation comparable with published values. This method supports investigating reentry plasma properties from signal attenuation.

ACKNOWLEDGMENT

The author thanks Gregg Radtke and Matthew Young for their helpful comments.

REFERENCES

[1] M.A. Heald, and C.G. Wharton, *Plasma Diagnostics with Microwaves*, John Wiley and Sons, Inc, New York, 1965, pp. 6-12

[2] A. Piel, *Plasma Physics An Introduction to Laboratory, Space, and Fusion Plasmas*, Springer-Verlag Berlin Heidelberg, 2010, pp 143-144

[3] T.C. Lin, L.K. Sproul, D.W. Hall, and J. Sontowski, "Reentry Plasma Effects on Electromagnetic Wave Propagation", 26th AIAA Plasmadynamics and Lasers Conference, June 19-22, 1995, AIAA 95-1942.

[4] T.C. Lin and L.K. Sproul, "Influence of reenrtry turbulent plasma flucation on EM wave propagation", *Computers & Fluids* 35 (2006) 703-711.

[5] J.P. Rybak and R.J. Churchill, "Progress in Reentry Communications", *IEEE Trans. on Aerospace and Electronics Systems*, Vol. AES-7, No. 5, September 1971.

[6] R.E. Kiel, R.F. Bergeron Jr., T.J. Kessler and A.E. Kaplan, "Boundary-Layer Plasma of a Re-Entry Vehicle: A Comparison of Prediction Models and Flight Measurements", *AIAA J.*, Vol. 11, No. 9, September 1973.

[7] A. Demetriades and R. Grabow, "Mean and Fluctuating Electron Density in Equilibrium Turbulent Boundary Layers", *AIAA J.*, Vol. 9, No. 8, August 1971.

[8] W.T. Langan, J.D. Cresswell and W.G. Browne, "Effects of Ablation Products on Ionization in Hypersonic Wakes", *AIAA J.*, Vol. 3, No. 12, December 1965.

[9] J.J. Kane, "Nonequilibrium Sodium Ionization in Laminar Boundary Layers", *AIAA J. Tech. Notes, Vol. 2., No. 9, September 1964.*

[10] E. Josyula and W.F. Bailey, "Governing Equations for Weakly Ionized Plasma Flowfields of Aerospace Vehicles", *J. of Spacecraft and Rockets*, Vol. 40, No. 6, November-December 2003.

[11] G.V. Candler and R.W. MacCormack, "Computation of Weakly Ionzied Hypersonic Flows in Thermochemical Nonequilibrium", *J. Thermophysics*, Vol. 5, No. 3, July-Sept. 1991.

[12] F.G. Blottner, "Nonequilibrium Laminar Boundary-Layer Flow of Ionized Air", *AIAA J.*, Vol. 2, No. 11, November 1964.

[13] C.G. Watkins and F.G. Blottner, "Three-Dimensional Effects on Electron Density in a Blunt Body Laminar Boundary Layer", *AIAA J.*, Vol. 10, No. 10, October 1972.

[14] R. Savino, M.E. D'Elia, and V. Carandente, "Plasma Effect on Radiofrequency Communications for Lifting Reentry Vehicles", *J. of Spacecraft and Rockets*, Vol. 52, No. 2, March-April 2015.

[15] G. He, Y. Zhan, J. Zhang, and N. Ge, "Characterization of the Dynamic Effects of the Reentry Plasma Sheath on Electromagnetic Wave Propagation", *IEEE Trans. on Plasma Sci.* Vol. 44, No. 3, March 2016.

[16] Y. Takahasi, K. Yamada, and T. Abe, "Prediction Performance of Blackout and Plasma Attenuation in Atmospheric Reentry Demonstrator Mission", *J. of Spacecraft and Rockets*, Vol. 51, No. 6, November-December 2014.

[17] B. Bai, X. Li, Y. Liu, J. Xu, L. Shi, and K. Xie, "Effects of Reentry Plasma Sheath on the Polarization Properties of Obliquely Incident EM Waves", *IEEE Trans. on Plasma Sci.* Vol. 42, No. 10. October 2014.

[18] R. Rawhouser, "Overview of the AF Avionics Laboratory Reentry Electromagnetics Program," NASA, Washington, DC, USA, Tech. Rep. NASA/SP-252, 1971.

[19] A. Demetriades, and R. Grabow, "Mean and Fluctuating Electron Density in Equilibrium Turbulent Boundary Layers", *AIAA J.*, Vol. 9, No. 8, August 1971.

[20] M. A. Lieberman and A. J. Lichtenberg, *Principles of Plasma Discharges and Material Processing*, Wiley, 1994 pp. 93-94

[21] J. J. S. Shang, *Computational Electromagnetic-Aerodynamics*, IEEE-Wiley, 2016 pp. 32